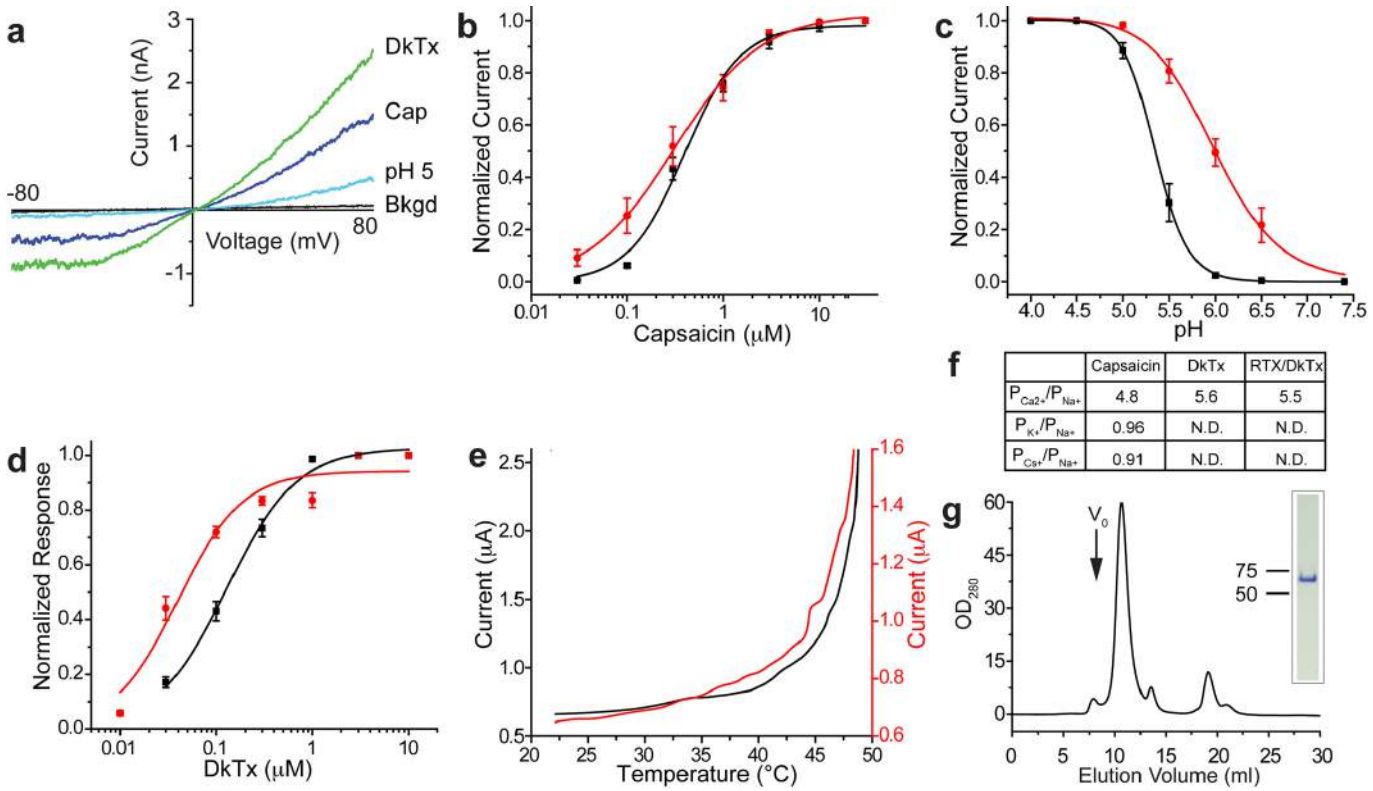

Extended Data Figure 1 | A minimal TRPV1 channel that is functional and biochemically stable. **a**, Mammalian (HEK293) cells expressing a minimal construct (with an N-terminal green fluorescent protein (GFP) tag) responded to various TRPV1 agonists, including capsaicin (Cap; 0.5 μM), extracellular protons (pH 5.0) and double-knot spider toxin (DkTx; 2 μM). Electrophysiological responses were measured in whole-cell patch-clamp configuration. **b**, **c**, Dose–responsive curves for capsaicin (**b**) or protons (**c**) were determined for minimal (black) or full-length (red) TRPV1, both of which contained an N-terminal GFP fusion. Values were normalized to maximal currents evoked by 30 μM capsaicin (**b**) or pH 4.0 (**c**) ($n = 6$ independent whole-cell recordings). **d**, DkTx dose–response curves for minimal (black) or full-length (red) TRPV1 as in **b** and **c**, determined by calcium imaging. Values were normalized to maximal capsaicin (10 μM)-evoked response in transfected HEK293 cells ($n > 30$ per point). **e**, Thermal response profiles for minimal (black) or full-length (red) TRPV1-expressing oocytes reveal similar heat sensitivity. **f**, Ion permeability ratios of agonist-evoked currents from minimal TRPV1 were estimated from reversal potential shifts in whole-cell patch-clamp recordings of transfected HEK293 cells, revealing no significant differences from full-length channel. **g**, Gel-filtration profile (Superdex-200) of detergent solubilized TRPV1 after purification on amylose affinity resin and proteolytic removal of maltose-binding protein (MBP) tag. The major species elutes as a symmetrical peak after the void volume (V_0). Inset shows that peak material migrates as a single, homogeneous band on SDS–PAGE (4–12% gradient gel; Coomassie stain).

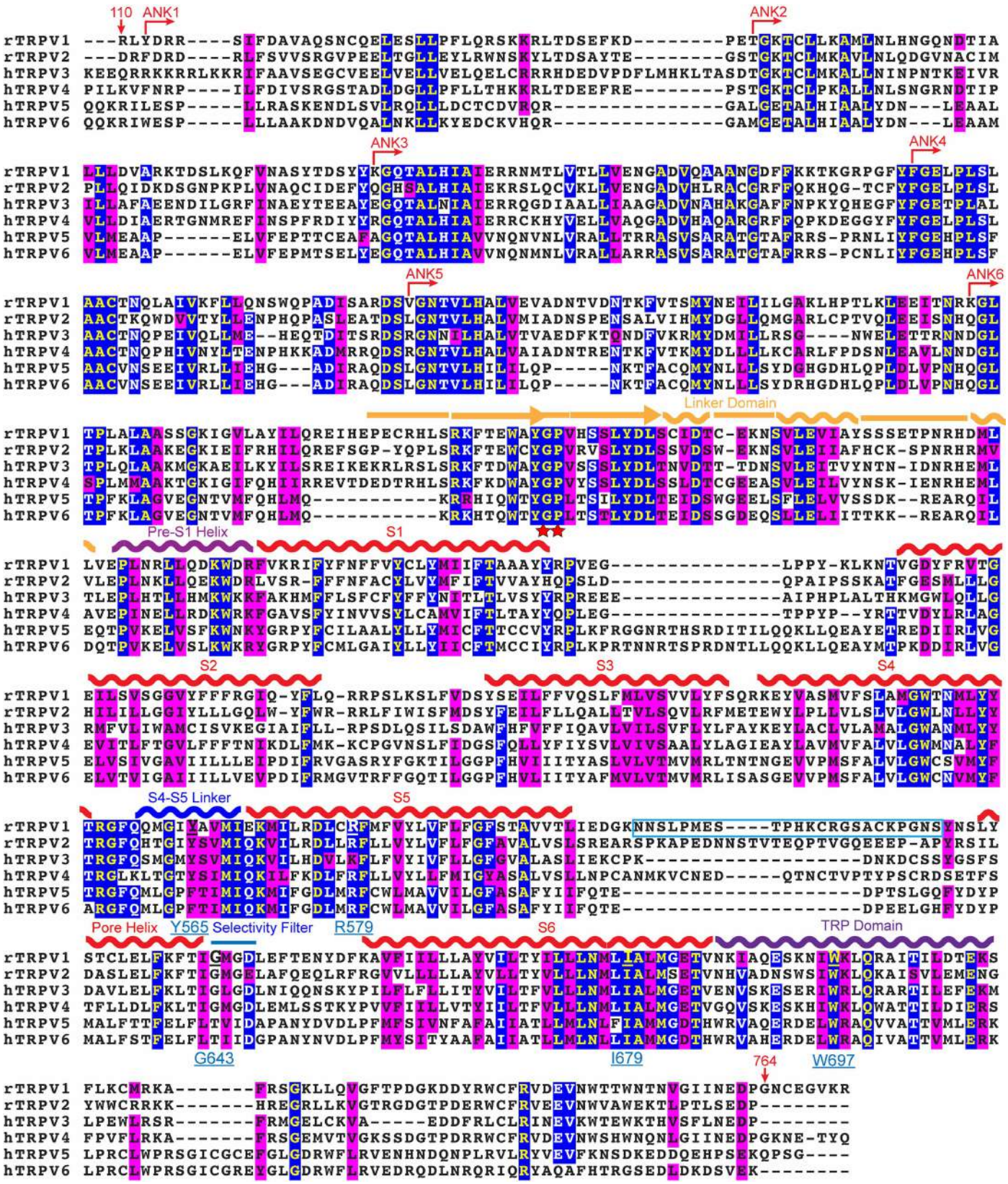

Extended Data Figure 2 | Sequence alignment of TRPV1 to other TRPV family members. The rat TRPV1 construct used for this study consists of residues 110 to 764 (indicated by red arrows), excluding the highly divergent region (604–626, highlighted by cyan box). Secondary structure elements are indicated above the sequence. The starting points of six ankyrin repeats are based on a crystal structure of ARD of TRPV1 (PDB 2PNN). Several critical residues discussed in the text are labelled in blue, and conserved glycine and proline residues at the turn of a β-sheet (highlighted in Fig. 6) are indicated with red stars.

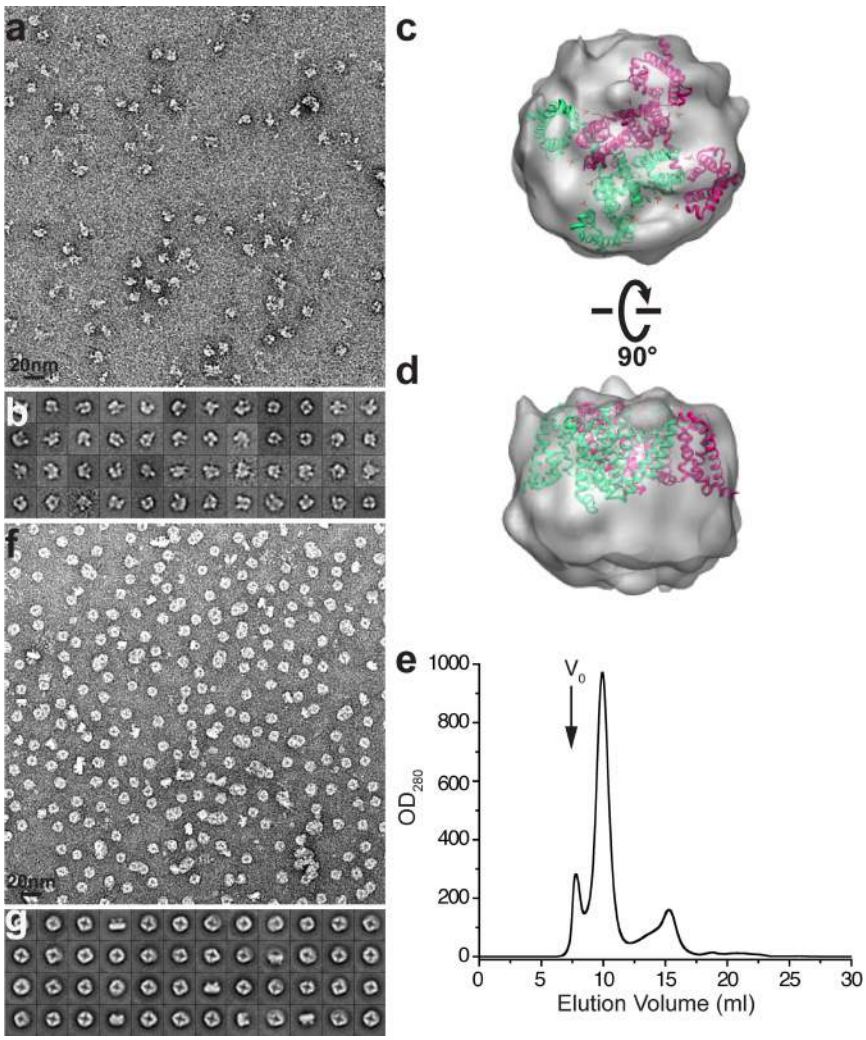

Extended Data Figure 3 | Negative-stain EM of TRPV1. **a**, Representative negative-stain image of purified minimal TRPV1 protein in detergent (n-dodecyl β-d-maltopyranoside; DDM) after proteolytic removal of MBP tag. **b**, 2D class averages of negatively stained particles in DDM. **c**, **d**, Two views of a random conical tilt (RCT) reconstruction from negatively stained TRPV1 in DDM. The RCT reconstruction was low-pass filtered at 30 Å, and fitted with the structure of Na_VAb (PDB 3RVY) to indicate the size and general shape. **e**, Gel-filtration profile (Superdex-200) of purified minimal TRPV1 protein after exchange from DDM into amphipols. The major species elutes as a symmetrical peak after the void volume (V_0). **f**, Representative negative-stain image of purified minimal TRPV1 protein without MBP tag in amphipols. **g**, 2D class averages of negative-stain particles in amphipols.

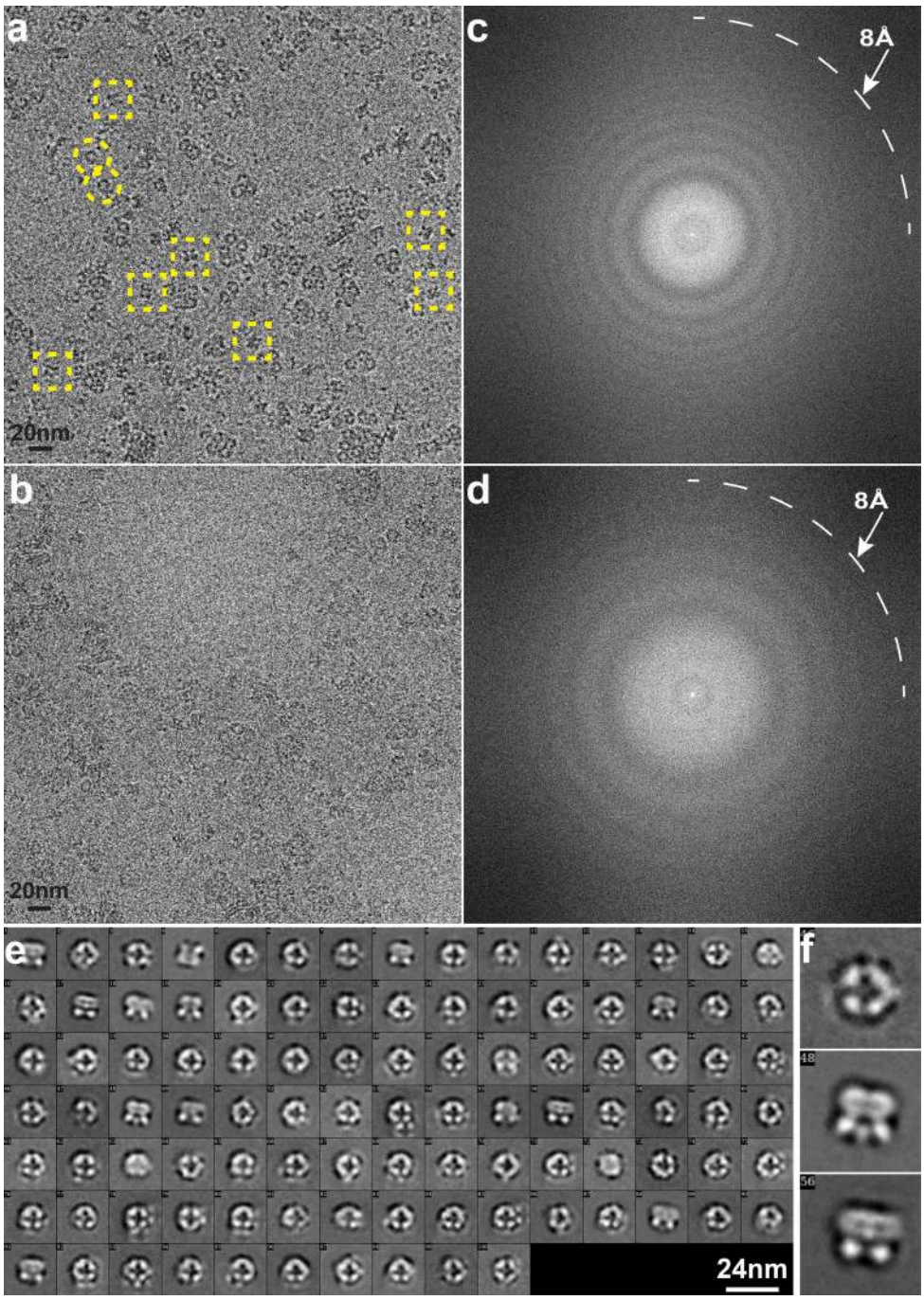

Extended Data Figure 4 | Cryo-EM of TRPV1 using Tecnai TF20 microscope and TemF816 8k × 8k CMOS camera. **a**–**d**, Representative images of frozen hydrated TRVP1 in amphipols taken at different defocus levels, 3.1 μm (**a**) and 1.5 μm (**b**) and their Fourier transforms (**c**, **d**). Thon rings extend to ~8 Å. Dash-line squares or circles indicate representative particles showing two distinctive views. **e**, 2D class averages of TRPV1 particles. **f**, Enlarged view of three representative 2D class averages.

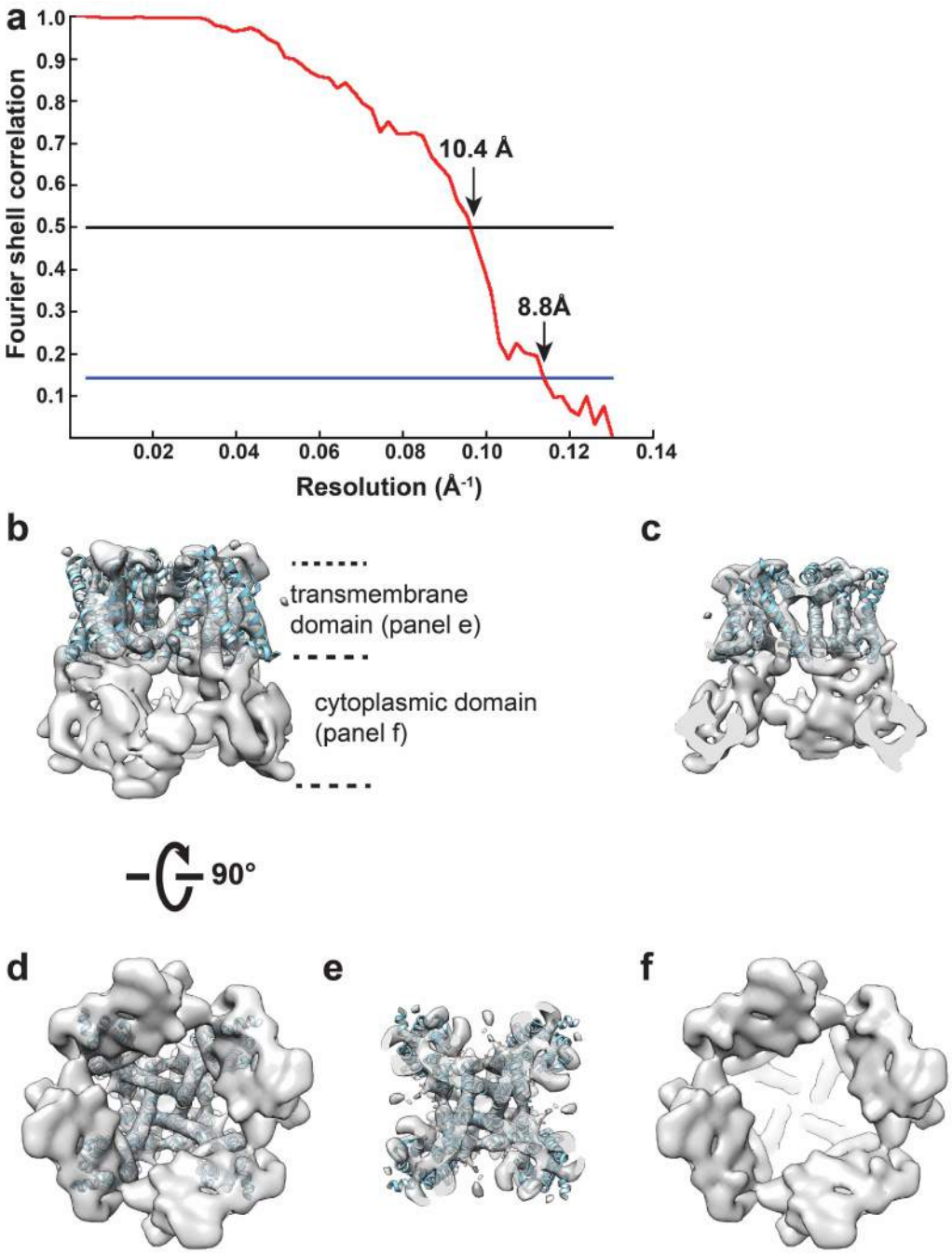

Extended Data Figure 5 | 3D reconstruction of TRPV1 calculated from TF20 data. **a**, Gold-standard FSC curve for the 3D reconstruction, marked with resolutions corresponding to FSC = 0.5 and 0.143. **b**, Side view of the 3D reconstruction low-pass filtered at 9 Å and amplified by a temperature factor −1,500 Å^2, showing transmembrane (top) and cytoplasmic (bottom) domains. The transmembrane domain roughly fitted by the atomic model of Na_VAb (PDB 3RVY). **c**, Longitudinal cross section view focused on central transmembrane helices. **d**, Bottom-up view of the 3D reconstruction shows overall structure. **e**, **f**, Bottom-up cross-section views showing the arrangement of transmembrane (**e**) and cytoplasmic (**f**) domains.

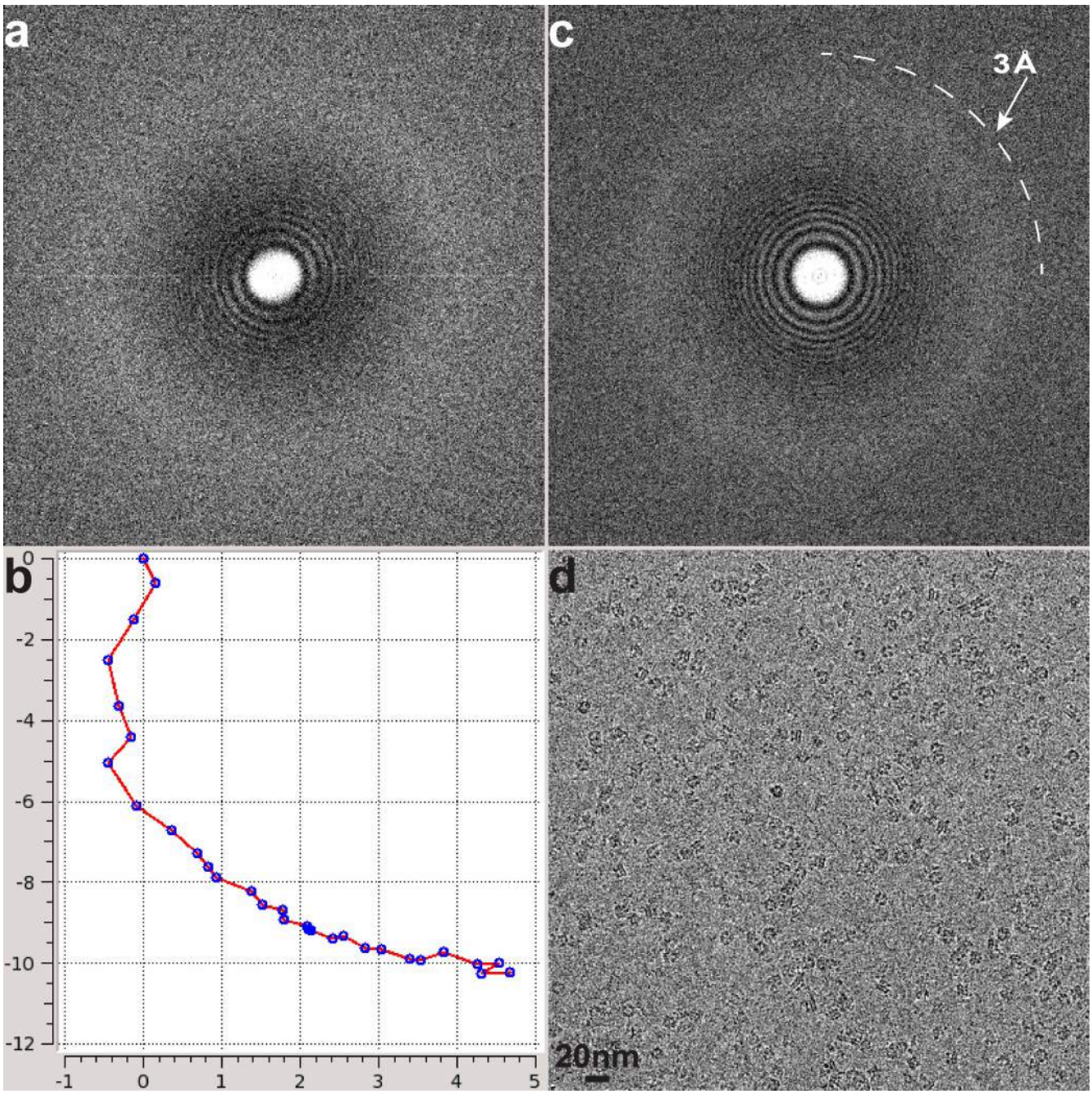

Extended Data Figure 6 | Motion correction improves the quality of images collected on Polora TF30 microscope using a K2 Summit direct electron detector. **a**, Fourier transform of a representative cryo-EM image of TRPV1 embedded in a thin layer of vitreous ice over Quantifoil hole without supporting carbon film before motion correction. **b**, Path of motion of 30 individual subframes, determined as described in Methods. **c**, **d**, A nearly perfect Fourier transform (**c**) was restored after the EM image was corrected for motion (**d**).

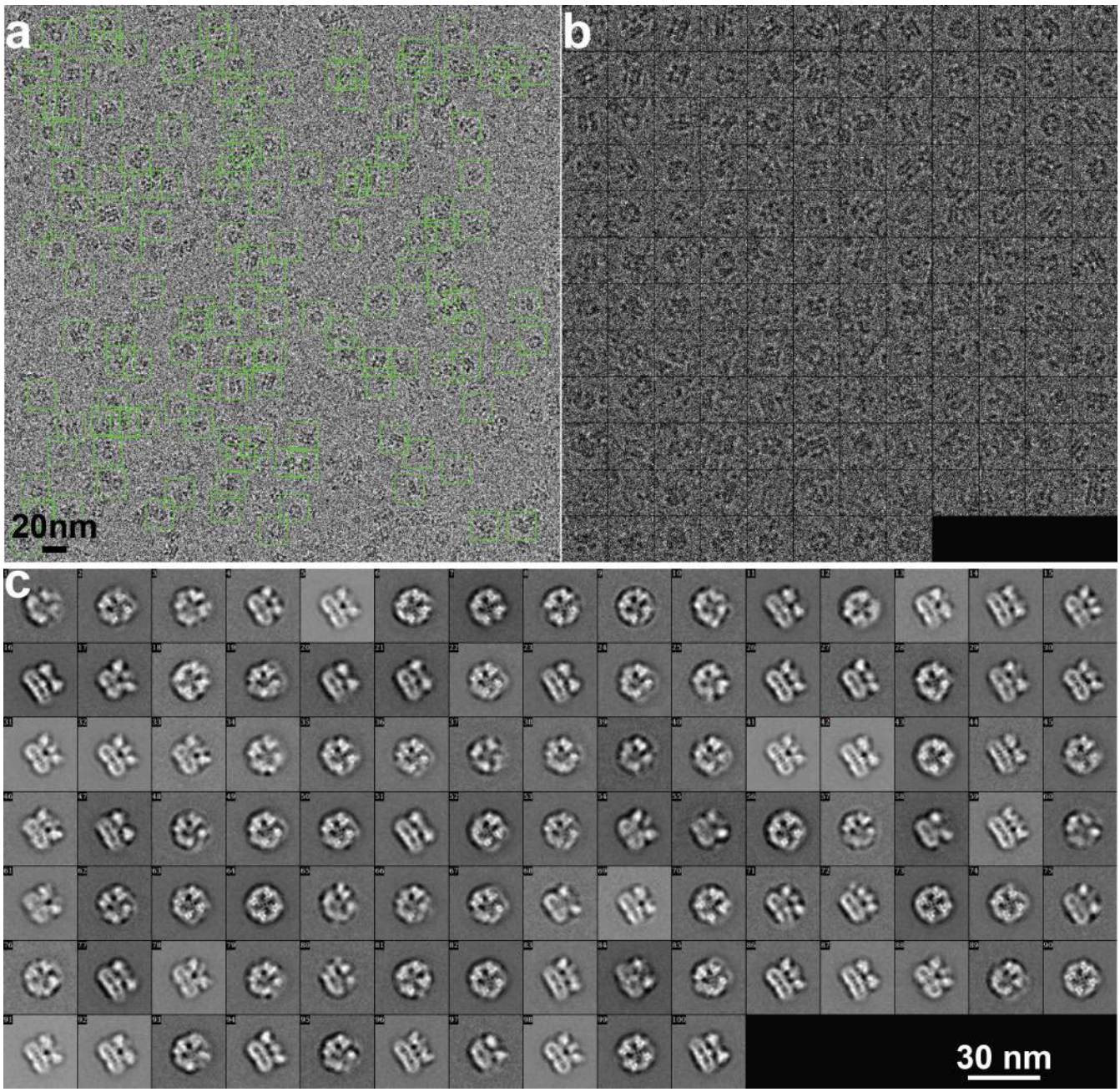

Extended Data Figure 7 | Picking and 2D classification of TRPV1 Cryo-EM particles collected on Polora TF30 microscope. **a**, Representative cryo-EM image after motion correction. Green boxes indicate all particles that were selected by semi-automatic particle picking and 2D screening, as described in Methods. **b**, Gallery view of the particles shown in **a**. **c**, 2D class averages of cryo-EM particles show many fine features (also seen in enlarged views in Fig. 1c), and these features are not visible in the 2D class averages of cryo-EM particles from TF20 data (Extended Data Fig. 4e, f).

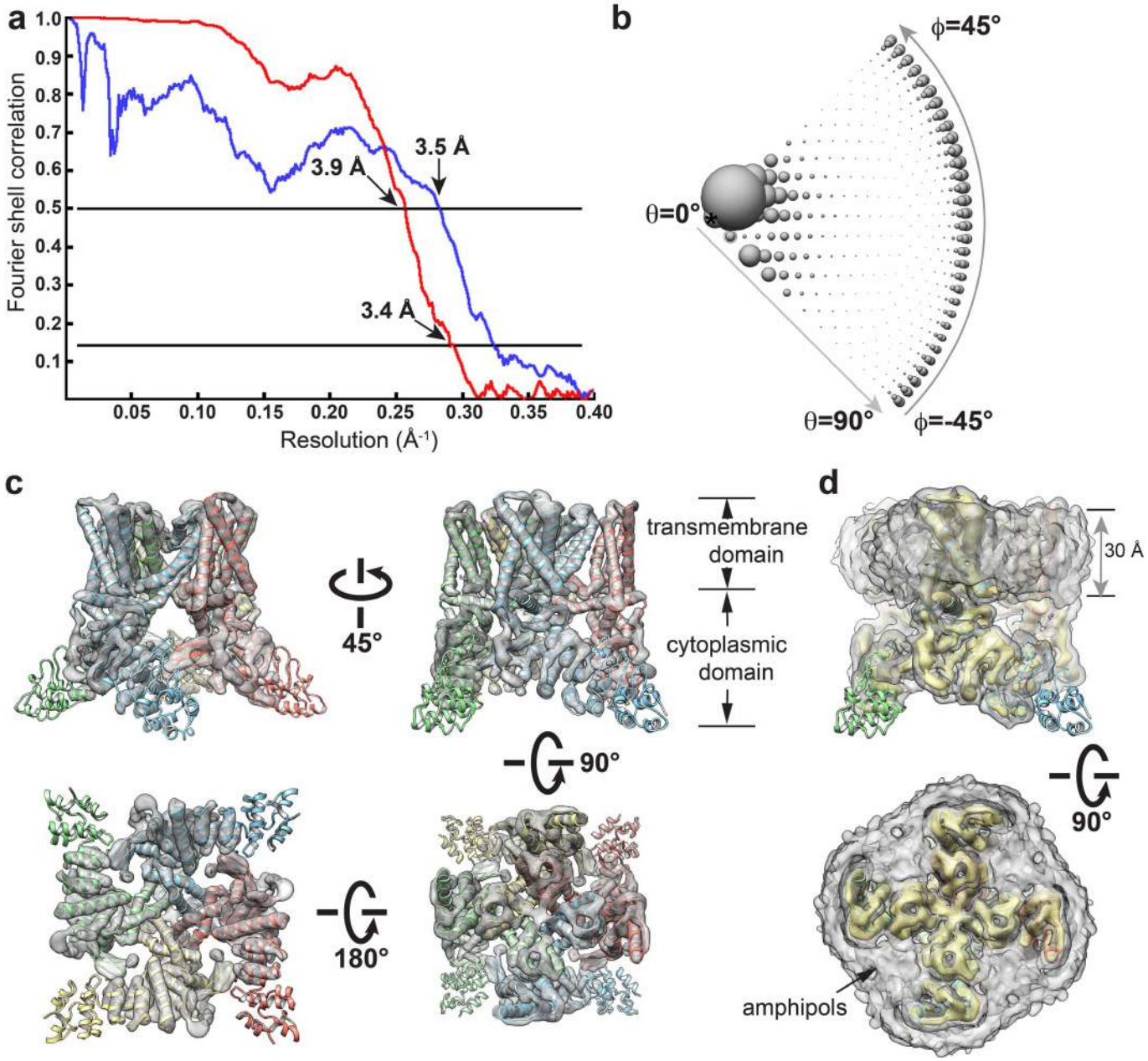

Extended Data Figure 8 | 3D reconstruction of TRPV1 calculated from TF30 data. **a**, Gold-standard FSC curve (red) of the final 3D reconstruction, marked with resolutions corresponding to FSC = 0.5 and 0.143. The FSC curve between the final map and that calculated from the atomic model is shown in blue. The relative low value of this FSC (blue) at low frequency range (>10 Å) is probably due to the presence of amphipol density in the experimental map. **b**, Euler angle distribution of all particles used for calculating the final 3D reconstruction. The sizes of balls represent the number of particles. The accuracy of rotation is 3.54°, as reported by RELION. **c**, Different views of the 3D reconstruction low-pass filtered at 6 Å and amplified by a temperature factor of −100 Å^2, fitted with the atomic model of TRPV1. **d**, Two views of the 3D reconstruction displayed at two different isosurface levels (high in yellow and low in grey). At the low isosurface level, the belt-shaped density of amphipols is visible with a thickness of ~30 Å.

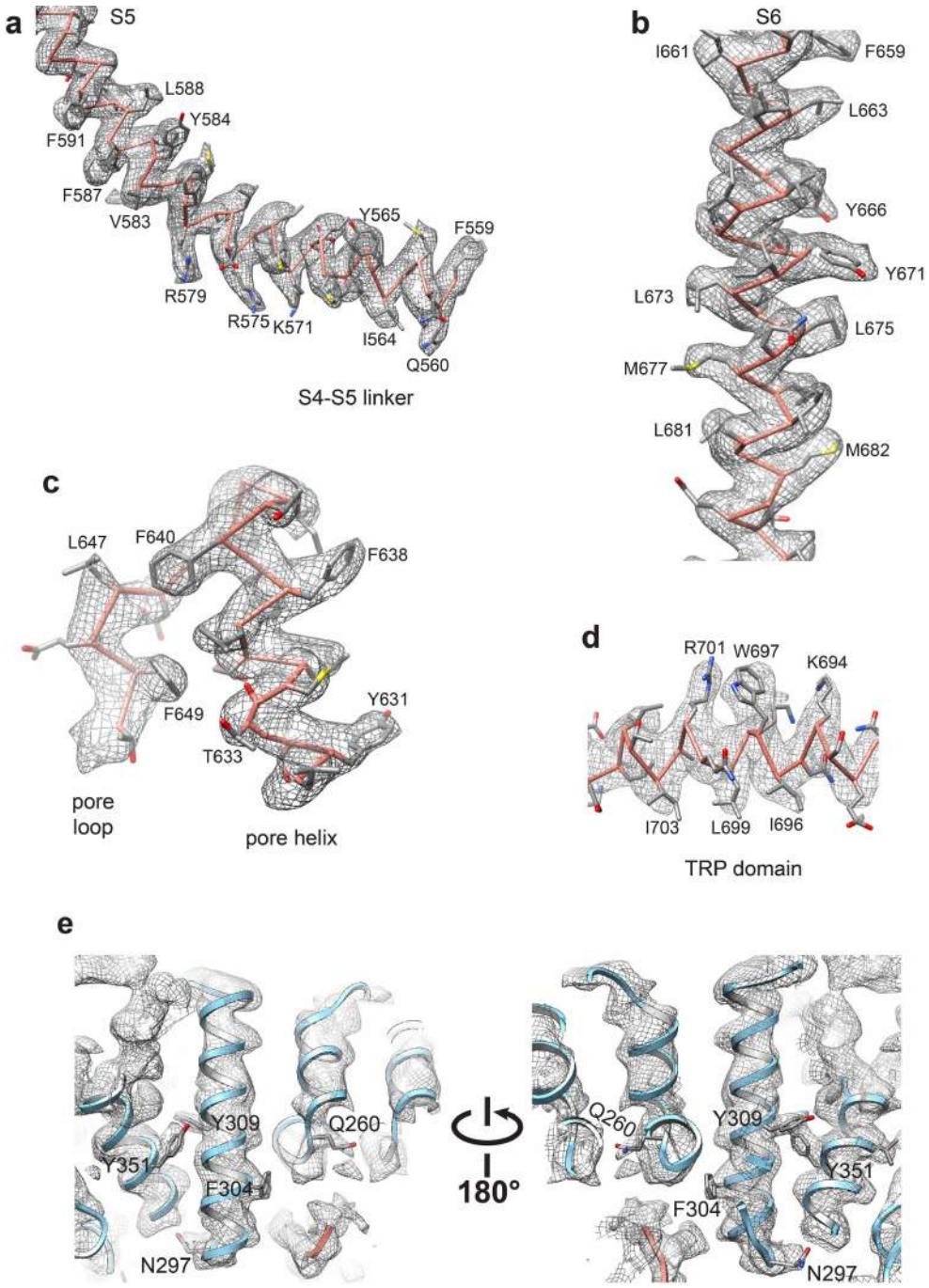

Extended Data Figure 9 | Cryo-EM densities of selected regions of TRPV1 at 3.4 Å resolution. **a**–**d**, Representative cryo-EM densities (grey mesh) are superimposed on atomic model (main chain in pink) for various TRPV1 domains, as indicated. **e**, **f**, Representative cryo-EM densities (grey mesh) are docked with crystal structure of TRPV1 ankyrin repeats (PDB 2PNN). Accuracy of docking was supported by fitting of several bulky side chains. Map was low-pass filtered to 3.4 Å and amplified by a temperature factor −100 Å^2.

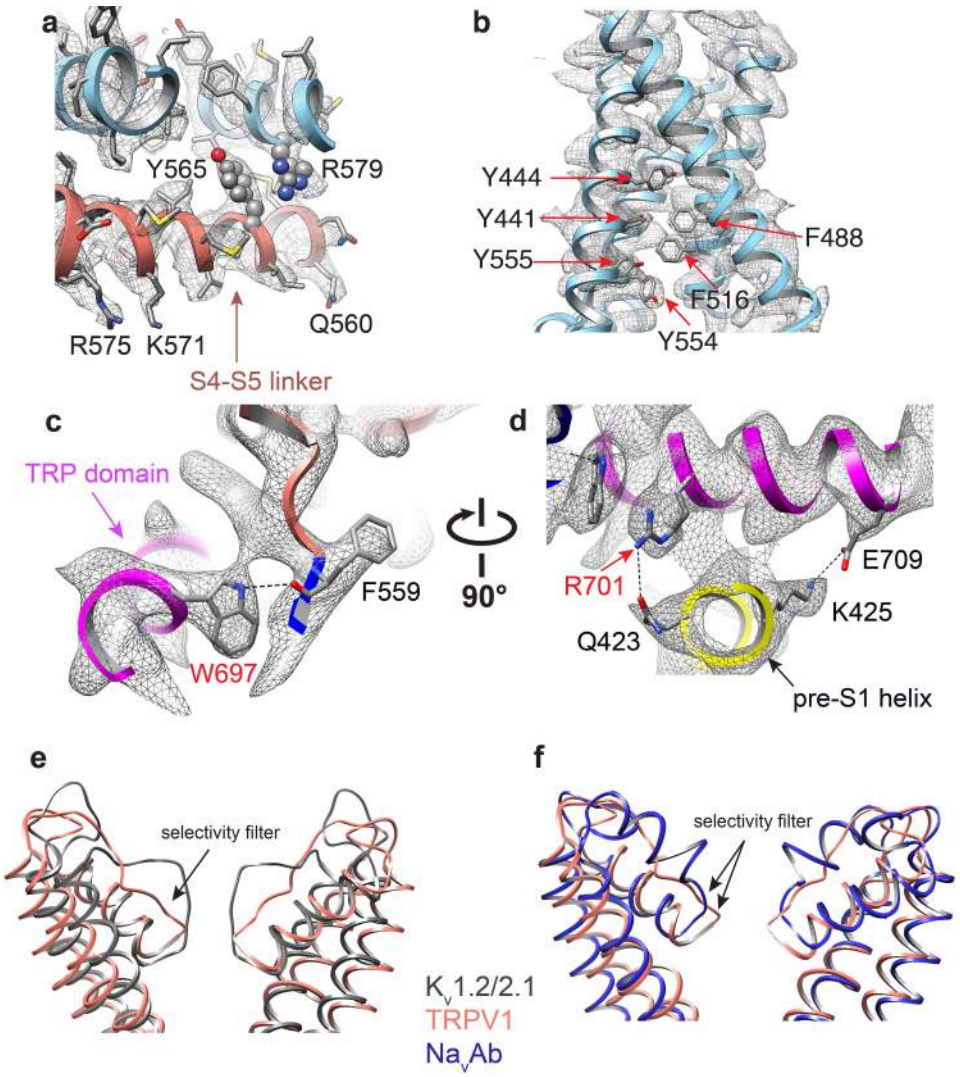

Extended Data Figure 10 | Details of domain interactions and outer pore configurations. **a**–**d**, Cryo-EM densities (grey mesh) of highlighted regions of TRPV1, as indicated, at 3.4 Å resolution are superimposed onto atomic model. Map was low-pass filtered to 3.4 Å and amplified by a temperature factor −100 Å^2. **e**, Superimposition of TRPV1 (salmon) with K_V 1.2–2.1 chimaera (PDB 2R9R; grey). **f**, Superimposition of TRPV1 (salmon) with Na_VAb (PDB 3RVY; blue). In each case, substantial structural differences are observed in the outer pore region. Structural alignments are based on the pore domain (S5–P–S6).